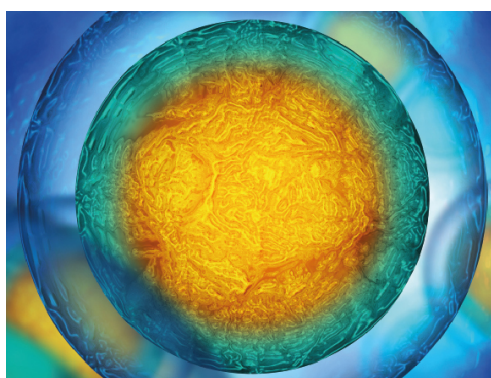


PAPER • OPEN ACCESS

Printability study of metal ion crosslinked PEG-catechol based inks

To cite this article: Magorzata K Wodarczyk-Biegun *et al* 2020 *Biofabrication* **12** 035009

View the [article online](#) for updates and enhancements.



Biophysical Society

IOP | ebooks™

Your publishing choice in all areas of biophysics research.

Start exploring the collection—download the first chapter of every title for free.

Biofabrication



PAPER

Printability study of metal ion crosslinked PEG-catechol based inks

OPEN ACCESS

RECEIVED

15 March 2019

REVISED

22 November 2019

ACCEPTED FOR PUBLICATION

3 January 2020

PUBLISHED

22 April 2020

Original content from this work may be used under the terms of the [Creative Commons Attribution 3.0 licence](#).

Any further distribution of this work must maintain attribution to the author(s) and the title of the work, journal citation and DOI.



Małgorzata K Włodarczyk-Biegun^{1,3} , Julieta I Paez¹ , Maria Villiou^{1,2} , Jun Feng^{1,2} and Aranzazu del Campo^{1,2,3}

¹ Leibniz Institute for New Materials, Campus D2 2, 66123 Saarbrücken, Germany

² Chemistry Department, Saarland University, 66123 Saarbrücken, Germany

³ Authors to whom any correspondence should be addressed.

E-mail: m.k.wlodarczyk@rug.nl and Aranzazu.DelCampo@leibniz-inm.de

Keywords: 3D printing, dynamic crosslinking, reversible network, PEG-catechol, metal-ligand coordination

Supplementary material for this article is available [online](#)

Abstract

In this paper we explore the printability of reversible networks formed by catechol functionalized PEG solutions and metal cations (Al^{3+} , Fe^{3+} or V^{3+}). The printability and shape fidelity were dependent on the ink composition (metal ion type, pH, PEG molecular weight) and printing parameters (extrusion pressure and printing speed). The relaxation time, recovery rate and viscosity of the inks were analyzed in rheology studies and correlated with thermodynamic and ligand exchange kinetic constants of the dynamic bonds and the printing performance (i.e. shape fidelity of the printed structures). The relevance of the relaxation time and ligand exchange kinetics for printability was demonstrated. Cells seeded on the materials crosslinked with Al^{3+} , Fe^{3+} ions were viable and revealed well-spread morphologies during 7 day culture, indicating the potential of the formulations to be used as inks for cell encapsulation. The proposed dynamic ink design offers significant flexibility for 3D bioprinting, and enables straightforward adjustment of the printable formulation to meet application-specific needs.

1. Introduction

Hydrogels are commonly used in 3D extrusion bioprinting [1]. They allow us to mimic the mechanical properties and hydration of biological tissues and show reasonable biocompatibility for cell encapsulation [2]. However, a typical hydrogel formulation used for cell encapsulation is not necessarily printable [2, 3]. A good hydrogel for 3D bioprinting needs to be easily extruded and to solidify quickly upon deposition. These abilities determine the accuracy and reproducibility of the printed structures, the time required for printing, and the resolution of the printed object [1]. Additionally, the required printing parameters (velocity, pressure), crosslinking chemistry and precursors should be compatible with living cells. Reactive hydrogels used for 3D printing make use of crosslinking agents [2, 4] or photo-polymerization of acrylate functional groups [4] for fast gelation. However, mixtures of fast reactive species typically result in narrow printability windows and low processability [3] due to limited control over the kinetics of the

crosslinking reaction [5]. Fast reactions lead to inhomogeneity of the printed structures, whereas slow kinetics lead to prints with poor shape fidelity [4]; photopolymerization after or during printing may lead to uneven irradiation doses in consecutively printed layers. For cellular ink formulations, fast crosslinking reactions or photopolymerization carry the risk of cell damage [6], whereas slow gelation is connected with cell sedimentation and uneven cell distribution in the final scaffolds [7].

A promising approach for printing hydrogels is the use of networks with reversible bonds. Reported examples make use of ionic interactions (e.g. alginate with calcium ions [8]), dynamic covalent bonds (e.g. hydrazone crosslinks [9]), guest-host complexes [10], hydrogen bonds [11], or metal-ligand coordination complexes [3, 12]. Networks with reversible bonds have several advantages over non-reversible systems for printing: they possess inherent shear thinning and self-healing properties; they do not require exposure to harsh conditions (e.g. UV irradiation or reactive crosslinking agents); and they do not need the addition

of thickening agents to increase viscosity to facilitate extrusion [4]. Among reversible bonds, metal-ligand coordination complexes offer wide versatility in terms of bonding strength and bonding dynamics by varying the metal ion or the pH of the system [3], leading to networks with adjustable mechanical properties [12]. Metal complexation is widely used in natural materials to tune mechanical strength of bulk and interface materials [3]. One of the most prominent examples is the metal-catechol interaction in the DOPA-rich mussel adhesive proteins. The catechol-metal interaction takes place in seawater due to the mild basic pH and the presence of metal ions, and leads to fast gelation of the secreted proteinaceous fluid. In a similar way, catechol-functionalized polymers mixed with metal ions (V^{3+} , Fe^{3+} , Al^{3+}) have been demonstrated to show pH-tunable crosslinking degree, fast network formation and self-healing behavior [13, 14]. The mechanical properties (e.g. shear modulus, relaxation time) of the formed polymer network can be finely tuned by the type of metal ion and pH [14, 15].

Only a few reports have exploited metal-ligand coordination complexes to obtain printable hydrogels [3, 12, 16]. The bisphosphonate- Ca^{2+} interaction has been used to print bisphosphonate-functionalized hyaluronic acid (HA-BP) at pH 7 [12]. The reversible gel composed by 2.7% w/v HA-BP and 200 mM $CaCl_2$ was printable and scaffolds with four layers with strand diameter of ca. 1 mm were printed without the need of further crosslinking. The gels were stable in PBS solution at pH 7 for 1 day but softened and dissolved within hours at lower pH. This is due to the protonation of bisphosphonate at decreasing pH, and the weakening of bisphosphonate- Ca^{2+} coordination. Crosslinking with Ag^{2+} was tested as an alternative [17], however the printability was not assessed. In a different work, the carboxyl- Fe^{3+} interaction was used to stabilize poly(acrylamide-co-acrylic acid) printed structures by immersing the prints in the metal ion salt, leading to robust gel formation [3]. Strands with diameter between 0.5–2 mm were obtained by extrusion of a 13% w/v polymer solution. The remarkable mechanical properties of the gel originated from the high polymer content, the broad range of coordination complexes and the stabilizing ionic interactions between carboxyl and amino groups. The strong carboxyl- Fe^{3+} association served as permanent crosslinks and provided gel integrity and high stiffness, whereas the weaker complexes served as reversible bonds, dissipating energy, and contributing to gel toughness. The influence of acrylic acid unit density and metal ion type and concentration on gel formation was tested. Crosslinking with Al^{3+} , Mg^{2+} , Ca^{2+} , Zn^{2+} , Ni^{2+} was attempted, but only mixing with Al^{3+} and Fe^{3+} led to gel formation, with significantly stronger gels obtained by crosslinking with Fe^{3+} ions. This effect was assigned to the highest coordination strength and stability of the carboxyl- Fe^{3+} interaction. Finally, the influence of pH on the coordination state

and stability constant of the complexes was investigated as a tool to introduce pH-driven tunability of mechanical properties, shape memory properties and sol-gel transition. Incorporation of sodium alginate (SA) to the polymer mixture lead to printed polymers with improved mechanical stability [16] where Fe^{3+} ions crosslinked with the carboxyl groups from both polymers. However, in order to achieve printable formulations, 10% silicone had to be added to the SA/P (AAm-co-AAc) mixture in order to obtain viscous prepolymer mixtures that could be extruded. In addition, a material deposition had to be followed by 10 min UV irradiation, 3 h of soaking in $Fe(NO_3)_3 \cdot 9H_2O$ solution, and 48 h incubation in water to remove excess of Fe^{3+} ions. With the proposed system prints with resolution limited to a strand size of $\sim 800 \mu m$ were obtained. However, the multiple and long processing steps make the system impracticable from an application point of view.

Here, we present printable polyethylene glycol (PEG) based formulations with catechol-metal complexes as reversible crosslinks that are able to support network formation at close-to-physiological pH and in the absence of harsh agents. The catechol-metal bonds serve as temporary crosslinks during printing, with the possibility of post-printing stabilization by gentle oxidation to form a covalent network. The inks can be printed without the use of a supportive bath or any additives to tune viscosity. No UV post-printing treatment is necessary to further stabilize the printed structures. In addition, the reactivity of catechol groups allows effective fixing of the printed material to different surfaces, including natural surfaces or tissues, eventually in wet conditions [18]. This system complements the recent report by Burdick *et al* [11] utilizing gallols for short-term gelation via reversible hydrogen bonding, and slow, spontaneous oxidation for long-term stabilization of the printed scaffolds. Distinctively, the metal complexation approach in our system offers flexible and controlled tuning of viscosity and mechanical properties, and adjustable ink formulation for specific application demands, including the possibility of using different catechol-functionalized polymeric materials. Additionally, printing can be performed with a broad range of printing parameters (speeds and pressures) and smooth strands with distinctively small diameters can be obtained.

This article reports on the rheological properties and printability window of PEG-catechol based inks crosslinked with V^{3+} , Fe^{3+} , and Al^{3+} ions, highlighting possible relationships between rheological parameters, thermodynamic and kinetic properties of the metal-catechol bond and printing results at different printing conditions. This study complements current efforts to correlate rheological behavior and printability of hydrogel-based inks [19–24], and contributes to the progress in the design and formulation of advanced inks.

Table 1. Composition and final pH of all the ink formulations used in the study.

Ink abbreviation	MW of PEG-Dop	Crosslinker	Final NaOH concentration	Final pH
PEG-Dop/Al³⁺	10 kDa	AlCl₃	33 mM	8.9
PEG-Dop/Al ³⁺ (pH 8.4)	10 kDa	AlCl ₃	30 mM	8.4
PEG-Dop/Fe³⁺	10 kDa	FeCl₃	33 mM	8.9
PEG-Dop/Fe ³⁺ (20 kDa)	20 kDa	FeCl ₃	15 mM	8.6
PEG-Dop/V³⁺	10 kDa	VCl₃	33 mM	8.6

*Main samples discussed in the study are indicated in bold. For detailed results obtained for PEG-Dop/Al³⁺ (pH 8.4) and PEG-Dop/Fe³⁺ (20 kDa) inks see supplementary information.

2. Materials and methods

2.1. Materials

We purchased 4-arm PEG succinimidyl carboxymethyl ester (PEG-NHS, Mw of 10, and 20 kDa) from Jenkem Technology (Plano, TX, USA). All other chemicals were purchased from Sigma-Aldrich (Germany), unless stated differently. Printing needles were provided by Vieweg (German), Optimum[®] cartridges and pistons for printing by Nordson (Germany).

2.2. Synthesis of PEG-Dopamine

Dopamine-functionalized PEG (PEG-Dop) was synthesized according to previously reported protocols [5, 18, 25]. 110 μ l of *N*-methylmorpholine (1.0 mmol) and 114 mg of dopamine (0.6 mmol) were mixed in 5.0 ml of anhydrous dimethylformamide (DMF) with magnetic stirring in argon atmosphere for 20 min. 1 g (0.1 mmol) of 4-arm PEG succinimidyl carboxymethyl ester (MW: 10 kDa) was dissolved in 5.0 ml of anhydrous DMF and was added dropwise into above mixture. The reaction was performed for 24 h at room temperature under Ar atmosphere, with constant stirring. After evaporation of DMF at reduced pressure, the crude product was redissolved in deionized water (pH 6.0) and dialyzed against deionized water (pH 6.0) with membrane tubing (MW cut-off of 3.5 kDa) for 2 days (dialysate was changed three times per day). The purified product was freeze dried and stored under -20°C until use. The obtained PEG-Dop was characterized by ¹H-NMR (Bruker Advance III HD, 300 MHz/54 mm, Fällanden, Switzerland) in D₂O to check the extent of the reaction and calculate the degree of catechol substitution. This was calculated by comparing the integral of the signal of PEG backbone (3.70–3.50 ppm which integrates for 220H or 440H for PEG with molecular weight 10 or 20 kDa, respectively) to the integral of the aromatic protons of dopamine (6.80–6.50 ppm, 3H). The obtained catechol substitution degree in all PEG batches was >85%.

2.3. Ink formulation

A 10% w/v solution of PEG-Dop (10 kDa or 20 kDa) in Milli-Q water was prepared and vortexed to ensure homogeneous mixing. Metal salt solutions at following concentrations were prepared in Milli-Q water: 40 mM FeCl₃, 40 mM AlCl₃ and 40 mM VCl₃. The

inks were prepared by mixing 1/2 final volume of PEG-Dop solution with 1/6 final volume of metal ion solution and, in the last step, 1/3 final volume of NaOH base (molarity indicated in table 1) in order to achieve homogenous cohesive networks. For example, to prepare 750 μ l of V³⁺-crosslinked PEG-Dop ink: 375 μ l of 10% w/v PEG-Dop, 125 μ l of 40 mM VCl₃ and 250 μ l of 100 mM NaOH were used. The sample was stirred with spatula in the Eppendorf tube until a homogenous sample was obtained. The final concentration of PEG-Dop in the samples was 5% w/v, and the molar ratio of dopamine to metal ions was 3:1. The pH of crosslinked network was measured with a pH-meter with flat surface electrode (PH100 Waterproof ExStik[®], Extech Instruments, USA). All the ink formulations used in this study are presented in table 1.

2.4. Rheological characterization

The rheological properties of PEG-Dop networks cross-linked with different metal ions (PEG-Dop/M³⁺) were measured using a rotational rheometer (DHR3, TA Instruments, USA) equipped with a 8 mm parallel plate geometry. A material volume of 8 μ l was used for the measurements. A measuring gap of 200 μ m was set and the experiments were performed at controlled temperature of 23 $^{\circ}\text{C}$. To avoid drying of the sample during testing, paraffin oil was applied around the samples after setting measuring gap and evaporation blocking cap was installed. All rheological experiments were performed at least in triplicate. For frequency test, two of six measurements conducted for PEG-Dop/Al³⁺ were excluded from the final data set, due to the one order of magnitude longer relaxation times than achieved in remaining four measurements.

2.4.1. Characterization of time dependent response and final stiffness

Frequency sweep oscillatory test was performed at 1% strain. The storage (G') and loss modulus (G'') were recorded over the frequency range of 10^{-2} to 10^2 Hz. The crossover modulus was taken as the modulus value at which G' intersects G'' . The relaxation time τ corresponded to the reciprocal of the frequency at which G' intersects G'' . The final material stiffness was analyzed by measuring G' and G'' as a function of time in an oscillatory test at a constant frequency ($f = 10$ Hz) and strain ($\gamma = 1\%$). After 180 s, the gels

were broken ($f = 10$ Hz and $\gamma = 0.01$ to 1000%) to monitor self-healing behavior. Subsequent gel reformation was analyzed for 1 h at constant frequency ($f = 10$ Hz) and strain ($\gamma = 1\%$). All tests were initiated 20 min after sample loading to the rheometer.

2.4.2. Characterization of shear thinning

The viscosity measurements were performed in the rotational flow sweep experiments. The same samples were used as for the frequency sweep oscillatory test. After 20 min of a soak time (to heal after oscillatory test), viscosity was recorded during the increasing shear rate $\dot{\gamma} = 0.001 \cdot 1/s$ to $3000 \cdot 1/s$ (shear rate given at the edge of the rotating plate).

2.5. Evaluation of printability

2.5.1. Filaments printing and characterization

PEG-metal inks were printed using pneumatic extrusion-based BioScaffolder 3.1 (GeSiM, Germany). For all experiments a 25 G conical nozzle (inner diameter: $260 \mu\text{m}$) was used. Extrusion pressure was in the range of 15–550 kPa (18 different levels, table S4) and the speed of printing head was set to 1, 2, 5 or 10 mm s^{-1} . The inks were prepared freshly before printing, loaded to 10 ml cartridges, closed with pistons to prevent leaking and ensure laminar ink flow, and after 20 min waiting time printed at room temperature into polystyrene 6-well cell culture plate placed on the holder on the printing stage. Each structure was imaged immediately after printing with stereomicroscope SMZ800N (Nikon, Germany) with home-made bottom illumination. Strand width was measured (nine measurements per sample) with the integrated NIS-Elements D (Nikon, German) software.

2.5.2. Printing in 3D

Crosslinking solution was prepared by mixing 50 ml of 36 mM sodium periodate (NaIO_4) with 30 ml MiliQ water and 20 ml 100 mM NaOH, to obtain an oxidizing solution with final oxidant concentrations of 18 mM NaIO_4 and pH ~ 9 .

PEG-Dop 3-dimensional multilayer grid-like constructs were printed based on the square design with $1 \text{ cm} \times 1 \text{ cm}$ dimensions (for PEG-Dop/ V^{3+}) or $9.1 \text{ cm} \times 9.1 \text{ cm}$ (PEG-Dop/ Al^{3+} and PEG-Dop/ Fe^{3+}), and consecutive layers rotated by 90° . After printing of each layer, ca. 2 ml of crosslinking solution was applied for 30 s on top of the print to introduce covalent crosslinking, and removed before printing of the next layer. For a PEG-Dop/ Al^{3+} , 1–4 layers constructs were printed with 85 kPa pressure and 3 mm s^{-1} printing speed. For a PEG-Dop/ Fe^{3+} , 1st layer was printed with 50 kPa pressure and 2 mm s^{-1} printing speed, all the consecutive layers were printed with 100 kPa pressure and 2 mm s^{-1} printing speed. For PEG-Dop/ V^{3+} , 1-layer construct was printed with 200 kPa pressure and 2 mm s^{-1} printing speed, 2–4 layers constructs were printed with 250 kPa pressure and 1 mm s^{-1} printing speed.

2.6. Cell studies

2.6.1. Cell culture

L929 Fibroblasts (ATCC, Germany) were cultured in RPMI 1640 medium (Gibco, 61870-010) supplemented with 10% FBS (Gibco, 10270), 200 mM L-glutamine and 1% penicillin/streptomycin (Invitrogen), at 37°C in a humidified atmosphere of 5% CO_2 . Cell culture media was changed every second day. Cells from passage 40–45 were used for short term studies and from passage 7–15 for long term studies.

2.6.2. Cell seeding

PEG-Dop/ M^{3+} mixtures were prepared as described in section 2.3. For short term analysis, samples of $30 \mu\text{l}$ of each ink type were molded into a 96-well plate. Half of the samples was used without subsequent treatment (metal-crosslinked samples), half was covered with $150 \mu\text{l}$ crosslinking solution (composition as in the section 2.5.2) for ca. 30 min (covalently crosslinked samples).

For longer term studies $60 \mu\text{l}$ and $80 \mu\text{l}$ of ink were molded in a 12 well chamber (Ibidi) or a 48-well plate, respectively. The gel was covalently functionalized with RGD cell adhesive peptide (for detailed procedure see SI).

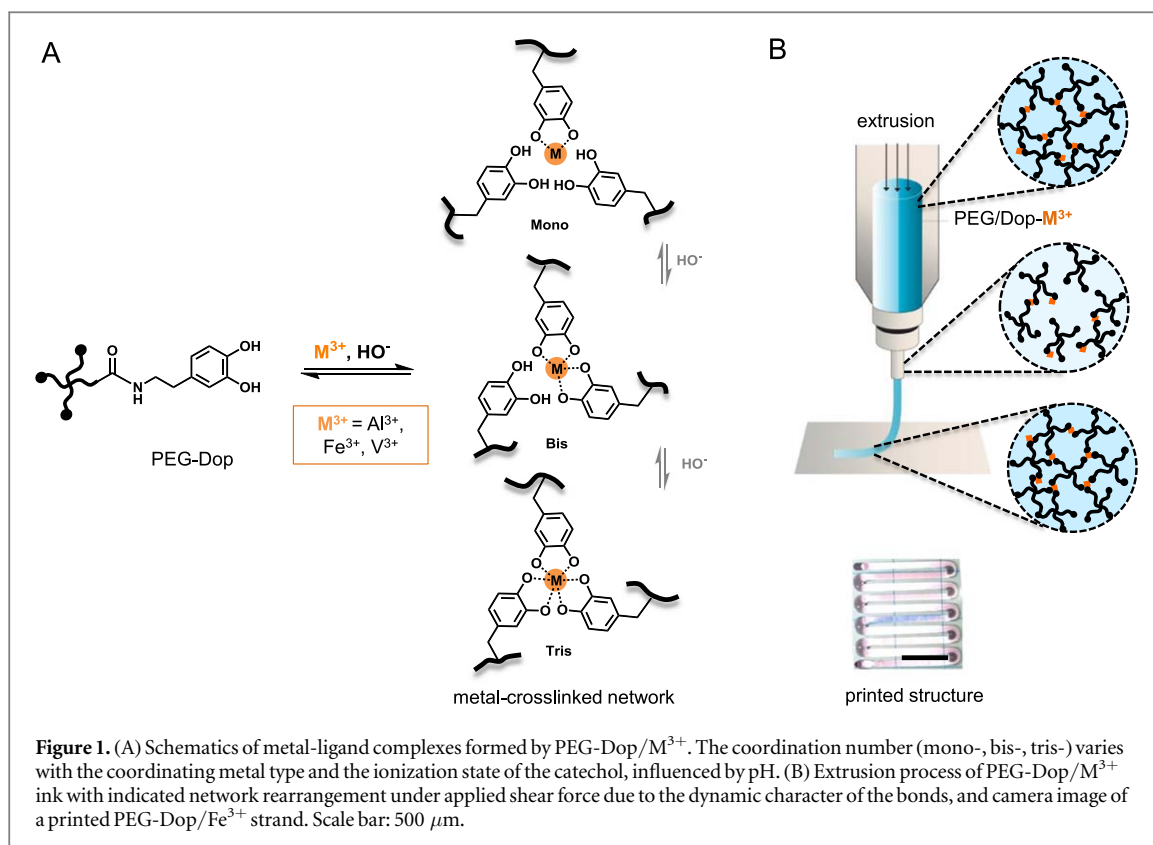
Samples were washed with $\sim 200 \mu\text{l}$ of medium prior to cell seeding (short term study) or three times with $250\text{--}500 \mu\text{l}$ of PBS (long term study) and seeded at the density $75\,000 \text{ cell cm}^{-2}$ (short term study) and $40\,000 \text{ cell cm}^{-2}$ (long term study). Samples were prepared in triplicates, with exception of PEG-Dop/ Al^{3+} at pH 8.9 in short term study (duplicate). The samples were incubated for 1 h at 37°C in a humidified atmosphere of 5% CO_2 up to 7 days. For long term study medium without phenol red (RPMI 1640, Gibco, 11835-030) was used (refreshed every 2–3 days), to avoid staining of the gel.

2.6.3. Live/dead assay

Staining protocol with fluorescein diacetate (FDA) to detect live cells and propidium iodide (PI) to detect dead cells, was used as follows. $1 \mu\text{g ml}^{-1}$ PI solution and $1 \mu\text{g ml}^{-1}$ FDA solution were dissolved in PBS to achieve final concentrations of $20 \mu\text{g ml}^{-1}$ and $6 \mu\text{g ml}^{-1}$, respectively. Cells were cultured on hydrogels for up to 7 days as indicated in the previous section. Cell culture medium was removed from the samples, and $100 \mu\text{l}\text{--}250 \mu\text{l}$ of staining solution was added to each well for 10 min. Samples were washed twice with PBS and imaged with PolScope microscope (Zeiss, Germany). Image analysis was performed with ImageJ software. If necessary background was subtracted, brightness and contrast adjusted, and counting of cells was performed with the function 'find maxima'.

2.6.4. Cell proliferation

Samples after 1, 4, and 7 days of culture were fixed with PFA 4% w/v for 10 min, washed three times in PBS,



permeabilized with 0.5% w/v Triton-X 100 (TX) for 10 min, and washed with PBS again. For nuclei visualization, samples were stained with 1:1000 DAPI (4',6-Diamidino-2-Phenylindole, Dihydrochloride, ThermoFisher) and washed with PBS. Imaging was performed using Nikon Ti-Eclipse (Nikon Instruments Europe B.V., Germany) with a Sola SE 365 II (Lumencor Inc., Beaverton, USA) solid state illumination device and an Andor Clara CCD camera for detection. As the gel samples were not flat, z-stuck images were captured. Image analysis was performed with ImageJ software: the function 'find maxima' was applied.

Additionally, Alamar Blue assay (Invitrogen) was used to compare cell metabolic activity at 1, 4, 7 days. According to manufacturer protocol, Alamar Blue reagent was dissolved in medium in 1:10 ratio, added to the samples and cells were incubated at 37 °C in a humidified atmosphere of 5% CO_2 for 3.5 h. Afterwards, medium was replaced with the fresh one and cell culture was continued till the next time point. The absorbance ($\lambda = 570 \text{ nm}$) of medium containing reagent was measured and compared to the fully reduced solution (medium with Alamar Blue after autoclaving at 120 °C for 15 min). In that way, the degree of reagent reduction by the cells was obtained as a measure of cellular activity. As it was noticed that the Alamar Blue treatment has negative effect on the cells growth (data not shown), only results from day 1 were used to compare cell activity on different scaffold types.

Table 2. Thermodynamic and kinetic parameters of catechol-metal coordination complexes: degree of coordination at pH 8.0, metal-catechol binding constant in tris-coordinated complexes, and water exchange rate constant.

Metal	Degree of coordination [15]	Log β_3	Water exchange rate constant: k [28]
Al^{3+}	Mono	41 ^a	1.92
Fe^{3+}	Bis	46,5 ^a /41 ^b	1.6×10^2
V^{3+}	Tris	40,5 ^b	5×10^2

^a Binding constant from [26], at 0.1 M KCl ionic strength and 25 °C.

^b Cumulative binding constant calculated based on [29].

2.7. Statistical analysis

All the results are reported as the mean \pm standard deviation. Statistical differences were analyzed based on one-way Analysis of Variance (ANOVA) performed using Excel Data Analysis or In Stat3 software. Differences for $p < 0.05$ were considered as significant.

3. Results

3.1. Ink development

PEG-Dop was mixed with the solutions of metal ions: Al^{3+} , Fe^{3+} , V^{3+} . The molar ratio of dopamine groups to metal ions was 3:1 in order to maximize the coordination degree of the complex. Since the solubility of metal cations is low at basic pH [14], the solutions of PEG-Dop polymer and cations were first

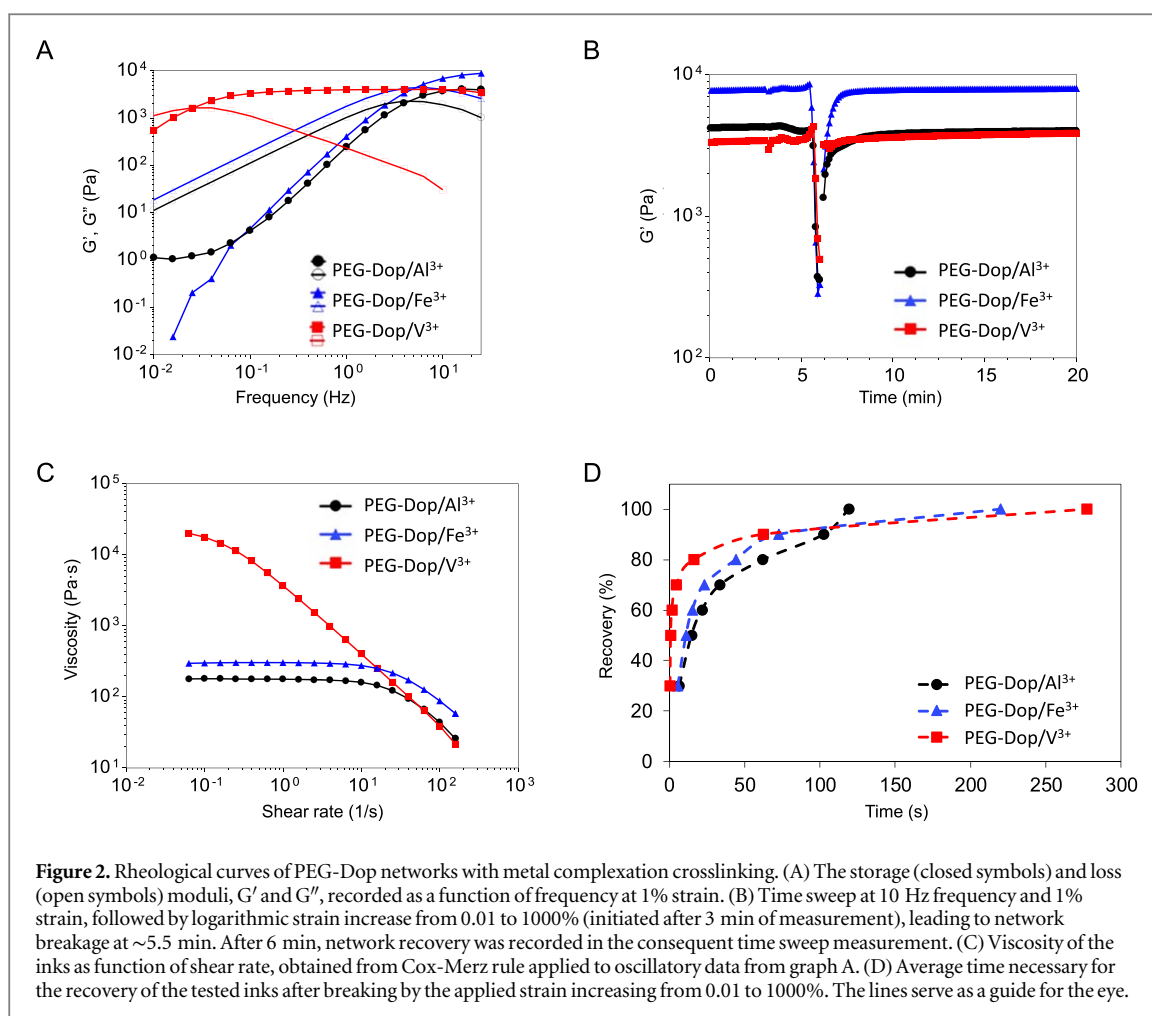


Table 3. Relaxation time and storage modulus of tested inks.

Ink	Relaxation time (τ) (s)	Storage modulus (G') (Pa) ^a
PEG-Dop/ Al^{3+}	0.23 ± 0.02	4020 ± 973
PEG-Dop/ Fe^{3+}	0.20 ± 0.06	7233 ± 1406
PEG-Dop/ V^{3+}	44 ± 19	2732 ± 1162

^a Measured at 10 Hz frequency and 1% strain.

mixed at acidic pH (pH 3–4) and then the pH was increased to pH 8.0 to allow complex formation. The immediate increase in viscosity at basic pH (and color change to purple and dark blue for PEG-Dop/ Fe^{3+} and PEG-Dop/ V^{3+} , respectively) indicated the fast formation of coordination bonds between the ionized catechol end-groups of the PEG-Dop chains and the metal ions (see figure 1 A for schematics of the metal-ligand complexation and table 2 for thermodynamic and kinetic parameters) [26, 27]. PEG-Dop/ V^{3+} formed crosslinked network almost instantly, while PEG-Dop/ Fe^{3+} and PEG-Dop/ Al^{3+} required longer time (in 10–20 s range) to form homogenous, viscous mixtures (slightly longer time for PEG-Dop/ Al^{3+} than PEG-Dop/ Fe^{3+}). Preliminary screening of PEG-Dop/ Fe^{3+} mixtures at different pH (pH 2.5–12.5) and polymer concentrations (2.5%, 5% and 10% w/v) was performed in order to

identify suitable ink compositions for extrusion printing. 5% w/v PEG-Dop (10 kDa) solutions at pH 8.6–8.9 gave the best results in terms of ink homogeneity and handling (for more details see supplementary information table S1 which is available online at stacks.iop.org/BF/12/035009/mmedia and figure S1). Table 1 presents the selected compositions from the preliminary screening, used for the printing experiments in the following sections. Figure 1(B) provides tentative representation of an extrusion process of the network with dynamic bonds.

3.2. Rheological evaluation of the PEG-Dop/ M^{3+} inks

The rheological properties of the material determine its suitability for printing. Frequency sweep measurements revealed liquid-like behavior of PEG-Dop inks crosslinked with Al^{3+} and Fe^{3+} , and predominantly solid-like behavior of PEG-Dop/ V^{3+} networks measured between 10^{-2} and 25 Hz (figure 2(A)). The G' and G'' curves crossed at 4.3, 5.5 and 0.025 Hz in PEG-Dop inks crosslinked with Al^{3+} , Fe^{3+} or V^{3+} respectively. These frequencies define the relaxation time of the networks, i.e. the time required to release an applied stress. Fe^{3+} and Al^{3+} crosslinked networks showed comparable relaxation times at pH 8.9, in the order of 0.2 s (table 3). The relaxation time did not

change with the molecular weight of the PEG-Dop (table S2), and was shorter at lower pH ($\tau = 0.12$ s for PEG-Dop/ Al^{3+} at pH 8.4, table S2). The PEG-Dop/ V^{3+} network showed the longest relaxation time ($\tau = 44$ s at pH 8.6). Previous studies have found relaxation times of ~ 0.09 s, 0.41 s and 7.6 s for 10 kDa 4-arm PEG-Dop hydrogel, with $\sim 15\%$ w/v polymer concentration, cross-linked with Al^{3+} , Fe^{3+} and V^{3+} , respectively, at pH 8.0 [15].

The stiffness of the networks and the ability to recover after damage at high strains was characterized in time by sweep experiments at frequency 10 Hz and 1% strain (figure 2(B)). The storage modulus G' of the network was higher for Fe^{3+} crosslinked networks (7 kPa) than for Al^{3+} and V^{3+} (4 and 3 kPa, respectively; see table 3). After breaking the network by high strains, the storage modulus dropped significantly (figure 2(B), drop in G' at $t = 5.5$ min), but the initial value of G' was recovered within a few minutes. The healing rate was evaluated as the time required to recover a certain percentage of initial G' value. Values are represented in figure 2(D). PEG-Dop/ V^{3+} showed the fastest healing rate, with 50% of initial G' value recovered in less than one second. PEG-Dop/ Al^{3+} and PEG-Dop/ Fe^{3+} showed 10-fold longer recovery times.

The shear thinning behavior of the inks was investigated during continuous rotation by monitoring the viscosity changes at increasing shear rate (figure S3(A)). However, measurements in rotational mode resulted in edge failure and material escape from the rheometer plates (see supplementary information, figure S3(B)). Therefore, the Cox-Merz rule was applied to the oscillatory data at small oscillations, as no escape of the material occurred (figure 2(C)). The Cox-Merz rule is an empirical relationship which allows to predict the shear-dependent viscosity based on the oscillatory data. The shear thinning data obtained with flow experiments corresponded to the ones obtained from the Cox-Merz rule, indicating applicability of the model (see supplementary information, figure S3(A)). Shear thinning in Fe^{3+} and Al^{3+} crosslinked networks was observed at shear rate above $10 \cdot 1/\text{s}$ (figure 2(C)). The shear thinning behavior was not affected by the molecular weight of the PEG-Dop, as tested in Fe^{3+} crosslinked polymer, or by a pH change to 8.4 in the Al^{3+} crosslinked polymer (figures S4(A), (B)). The V^{3+} crosslinked polymer showed shear thinning over the whole range of shear rate investigated (10^{-2} – $10^3 \cdot 1/\text{s}$), revealing earlier end of Newtonian plateau regime. As shown on figure 2(C), PEG-Dop/ V^{3+} was characterized by the highest zero shear viscosity (plateau observed at low shear rate), which indicates the highest resistance to deformation. For PEG-Dop/ V^{3+} the zero shear viscosity was expected to appear at rates $< 10^{-1} \cdot 1/\text{s}$ (figures 2(C) and S3), at the level of $20 \text{ kPa} \cdot \text{s}$. PEG-Dop/ Fe^{3+} and PEG-Dop/ Al^{3+} showed 2 orders of magnitude lower zero shear viscosity values ($\sim 200 \text{ Pa} \cdot \text{s}$).

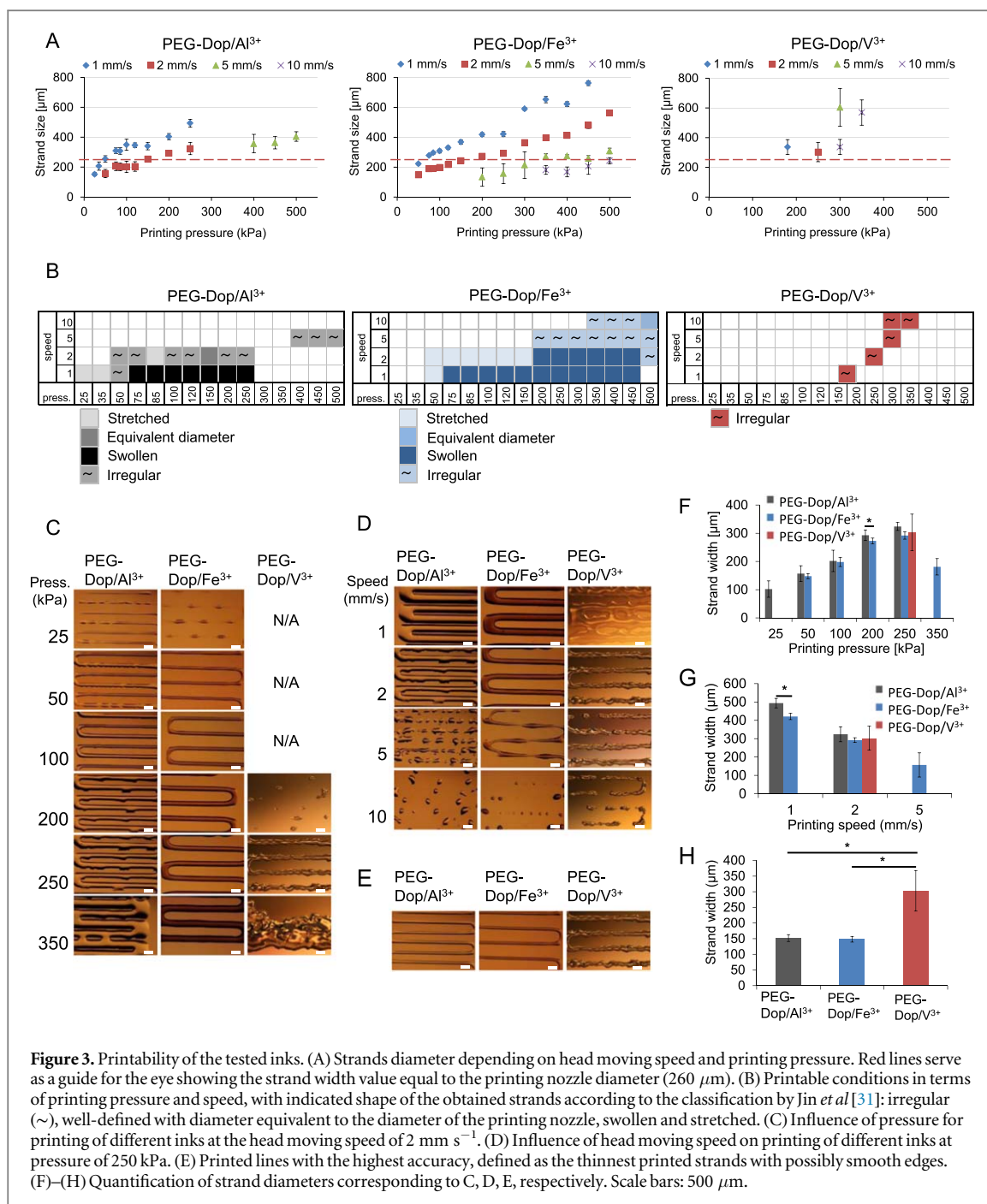
Based on reported procedures [20, 30] to obtain the theoretical shear rate and the apparent viscosity while printing, we calculated maximum shear rates that PEG-Dop/ M^{3+} experience during extrusion (for more details see supplementary information). Note that this calculation assumes that an ideal strand is printed (i.e. width of strand equal to needle diameter). Based on the calculations, maximum shear rates experienced during printing process are above $10 \cdot 1/\text{s}$. Therefore, the inks are expected to show shear thinning behavior at most of the printing conditions applied in this study (table S3). Additionally, the inks recovered their zero shear viscosity values when measured at $1/\text{s}$ shear rate, imitating material at rest, after applying higher shear rates ($10^2 \cdot 1/\text{s}$, imitating material while printing) (see figures S4(C)–(E)).

3.3. Filament printing

The printability of PEG-Dop networks crosslinked with different metals ions was evaluated. We used an extrusion printer with a $260 \mu\text{m}$ nozzle, and variable printing speed (1 – 10 mm s^{-1}) and printing pressure (50 – 500 kPa). We searched for the ‘printable window’ for each ink composition by identifying the printing parameters at which a continuous strand could be printed (including printed strands with rough or inconsistent edges). In order to characterize the strands we measured the filament width. All printed structures and the mean strand widths are presented in supplementary information (table S4).

5% w/v PEG-Dop formulations with Al^{3+} , Fe^{3+} and V^{3+} metal ions were printable, though the printing parameters were different for each PEG-Dop/ M^{3+} ink. PEG-Dop/ V^{3+} was only printable within a narrow range of printing conditions (figures 3(A), (B)). The printable window of PEG-Dop/ Al^{3+} was significantly broader, and PEG-Dop/ Fe^{3+} showed the broadest printability. Relatively high pressure was required for printing PEG-Dop/ V^{3+} , presumably due to its high viscosity. The results of theoretical calculations of inks apparent viscosity and shear rates while printing (for more information see supplementary information and table S3), corroborate the need of higher shear rates to extrude V^{3+} crosslinked ink.

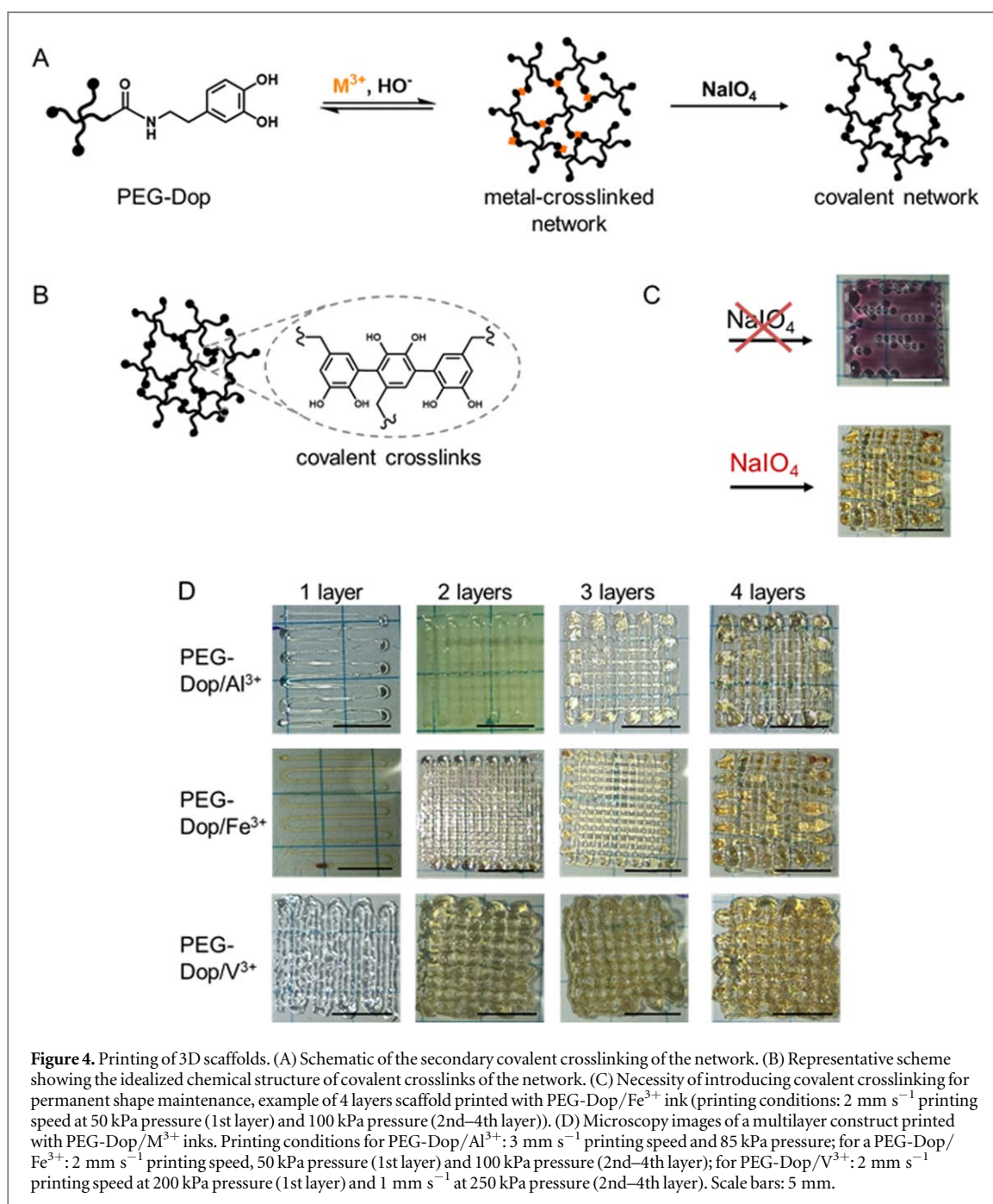
The filaments printed at the different conditions were imaged and classified as: well-defined or irregular, according to the classification proposed previously [31]. Irregular filaments include strands with rough surface, over-deposited, compressed or discontinuous; the last ones appearing as droplets or broken lines. The well-defined filaments were further classified as: filaments with equivalent diameter, when the filament has the same diameter as the printing nozzle, and as swollen or stretched filaments, if the diameter is bigger or smaller than the printing nozzle, respectively [31] (see figure 3(B) with marked filament type). Printed PEG-Dop/ V^{3+} filaments were irregular at all printing conditions (figures 3(C), (D)).



PEG-Dop/ Fe^{3+} rendered well-defined strands with diameter between $148 \pm 9\ \mu\text{m}$ and $762 \pm 16\ \mu\text{m}$ at printing pressures between 50 and $500\ \text{kPa}$, whereas PEG-Dop/ Al^{3+} formed well-defined strands with diameter between $152 \pm 11\ \mu\text{m}$ and $494 \pm 26\ \mu\text{m}$ within a narrower printing pressure range (25 – $250\ \text{kPa}$). Printed filaments of PEG-Dop/ Al^{3+} at pH 8.4 flowed and merged laterally within a significant range of tested conditions (figure S7).

The influence of printing pressure and printing speed on the width of the printed filaments is shown in figure 3. Increasing printing pressure resulted in wider strands (figures 3(C), (F)) which eventually merged. Using $2\ \text{mm s}^{-1}$ printing speed, strands of PEG-Dop/ Al^{3+} , PEG-Dop/ Fe^{3+} and PEG-Dop/ V^{3+} merged when the

printing pressure was $\geq 350\ \text{kPa}$, $\geq 450\ \text{kPa}$ and $\geq 350\ \text{kPa}$, respectively. Increasing printing speed resulted in thinner filaments, since the amount of deposited material per unit length decreased. At higher printing speeds ($5\ \text{mm s}^{-1}$ for PEG-Dop/ Al^{3+} but $10\ \text{mm s}^{-1}$ for PEG-Dop/ Fe^{3+} , at $250\ \text{kPa}$ printing pressure, figure 3(D)) the printed strands showed discontinuities. PEG-Dop/ Al^{3+} and/ Fe^{3+} printed filaments at the same speed and pressure showed similar filament width but different edge smoothness (compare figures 3(C)–(G)). PEG-Dop/ Al^{3+} (pH 8.4), with shorter relaxation time (figure S7), rendered significantly wider strand and the filaments merged more easily. If left without secondary crosslinking, all the printed structures fused eventually (figure 4(C)).



The thickness of the printed lines can be used as measurement of the accuracy of the printing process [20, 32]. The thinnest printed strand obtained using the nozzle of $260\ \mu\text{m}$ diameter was $148 \pm 9\ \mu\text{m}$, $152 \pm 11\ \mu\text{m}$ and $303 \pm 65\ \mu\text{m}$, for Fe^{3+} , Al^{3+} and V^{3+} crosslinked materials, respectively (figures 3(E), (H)). PEG-Dop/ Fe^{3+} ink showed the highest accuracy of the printed structures. Moreover, it also showed the broadest printability range and the smoothest printed structures.

3.4. Fabrication of multilayer constructs

The possibility to print 3D structures with PEG-Dop/ M^{3+} inks was explored. In order to increase the mechanical stability of the printed structures and allow 3D stacking of printed strands, a secondary

covalent crosslinking step by exposure to mild oxidizing conditions was implemented (figure 4). Figure 4(C) visualizes how 3D printed layers of filaments of PEG-Dop/ Fe^{3+} lose their shape within a few minutes after printing. Addition of an oxidant (sodium periodate) to each layer after printing led to a fast color change and fixation of the printed shape. This is attributed to the self-condensation of the oxidized catechol units to form mechanically stable threads [5] that do not collapse due to own weight. The representative bonds formed in covalent crosslinking are shown in figure 4(B) (see as well [33]). The change in color of the inks containing Al^{3+} , Fe^{3+} and V^{3+} from transparent, purple and dark blue respectively, to yellow/orange after treatment with sodium peroxide

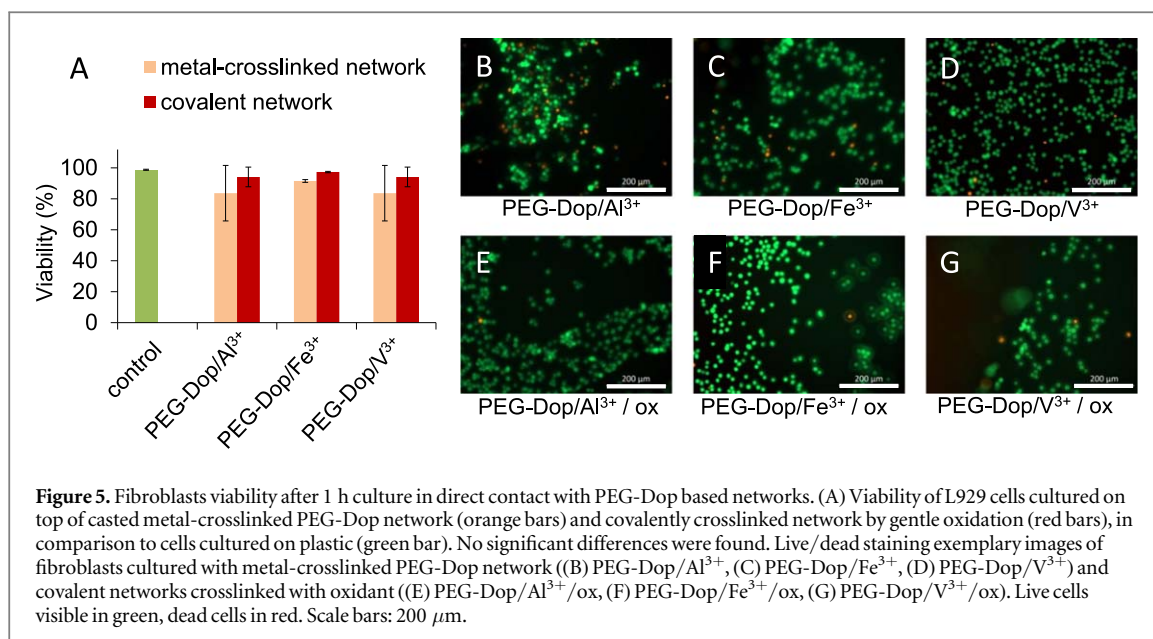


Figure 5. Fibroblasts viability after 1 h culture in direct contact with PEG-Dop based networks. (A) Viability of L929 cells cultured on top of casted metal-crosslinked PEG-Dop network (orange bars) and covalently crosslinked network by gentle oxidation (red bars), in comparison to cells cultured on plastic (green bar). No significant differences were found. Live/dead staining exemplary images of fibroblasts cultured with metal-crosslinked PEG-Dop network (B) PEG-Dop/Al³⁺, (C) PEG-Dop/Fe³⁺, (D) PEG-Dop/V³⁺ and covalent networks crosslinked with oxidant (E) PEG-Dop/Al³⁺/ox, (F) PEG-Dop/Fe³⁺/ox, (G) PEG-Dop/V³⁺/ox. Live cells visible in green, dead cells in red. Scale bars: 200 μ m.

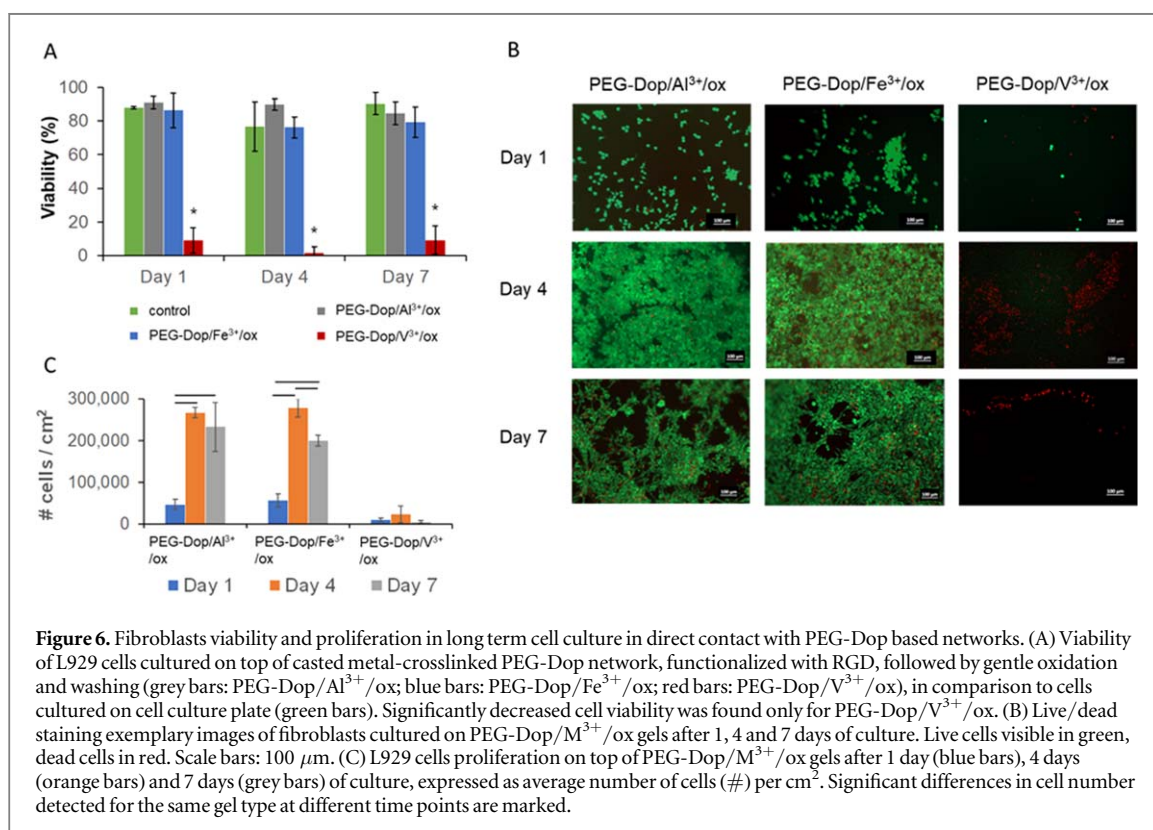


Figure 6. Fibroblasts viability and proliferation in long term cell culture in direct contact with PEG-Dop based networks. (A) Viability of L929 cells cultured on top of casted metal-crosslinked PEG-Dop network, functionalized with RGD, followed by gentle oxidation and washing (grey bars: PEG-Dop/Al³⁺/ox; blue bars: PEG-Dop/Fe³⁺/ox; red bars: PEG-Dop/V³⁺/ox), in comparison to cells cultured on cell culture plate (green bars). Significantly decreased cell viability was found only for PEG-Dop/V³⁺/ox. (B) Live/dead staining exemplary images of fibroblasts cultured on PEG-Dop/M³⁺/ox gels after 1, 4 and 7 days of culture. Live cells visible in green, dead cells in red. Scale bars: 100 μ m. (C) L929 cells proliferation on top of PEG-Dop/M³⁺/ox gels after 1 day (blue bars), 4 days (orange bars) and 7 days (grey bars) of culture, expressed as average number of cells (#) per cm². Significant differences in cell number detected for the same gel type at different time points are marked.

(figure 4(C)) confirms the presence of quinone oxidized species [14, 34].

1 \times 1 cm² mesh-like constructs consisting of up to four layers were successfully printed with PEG-Dop inks crosslinked with Fe³⁺, Al³⁺ and V³⁺ metal ions. Oxidative, covalent crosslinking was performed after deposition of each layer. The higher printing accuracy obtained with PEG-Dop/Fe³⁺ ink in previous experiments with 2D printed structures was also observed in 3D printed scaffolds (figure 4(D)). Additionally, to show the possibility of obtaining bulk 3D scaffolds, pyramid-like constructs consisting of three levels, 4–5

layers each, starting from a base area of \sim 1 cm² were printed (for more details see supplementary information, figure S8). Covalent crosslinking was performed after each deposited level. Constructs from PEG-Dop/Fe³⁺ and PEG-Dop/V³⁺ filaments maintained their shape, whereas PEG-Dop/Al³⁺ print collapsed.

3.5. Cell studies

The viability of cells grown on PEG-Dop networks with metal-coordination crosslinks and with covalent

crosslinks was evaluated in short (1 h) and long term studies (up to 7 days). Fibroblasts L929 were seeded on the top of casted PEG-Dop based networks. A live/dead assay showed high viability of the cells attached to all tested materials after initial 1 h of culture (figures 5 and S9). At later time points (1, 4 or 7 days) cells remained viable on the gels crosslinked with Al^{3+} and Fe^{3+} ions followed by covalent crosslinking (further denoted as: PEG-Dop/ Al^{3+} /ox and PEG-Dop/ Fe^{3+} /ox). Conversely, viability on the PEG-Dop/ V^{3+} /ox was significantly decreased (below 10% at day 1, day 4 and day 7) (figures 6(A), (B)). No statistical differences in viability were observed between cells cultured on the tissue plates (control) and on any of the tested inks, besides for PEG-Dop/ V^{3+} /ox in long term culture. Visible cell proliferation was observed from the life/dead assay images (figure 6(B)) and DAPI staining (figures 6(C) and S11) on the PEG-Dop/ Al^{3+} /ox and PEG-Dop/ Fe^{3+} /ox scaffolds. The cell density increased ca. 6 times between day 1 and day 4, followed by a small, but statistically significant, decrease at day 7 for PEG-Dop/ Fe^{3+} /ox. For PEG-Dop/ V^{3+} /ox gel, no cell proliferation was detected in long term study. Cells cultured on the PEG-Dop/ Al^{3+} /ox and PEG-Dop/ Fe^{3+} /ox scaffolds revealed spread morphology already at day 1, whereas on the PEG-Dop/ V^{3+} /ox scaffolds cells stayed round at all time points (figures 6(B) and S11). The Alamar Blue assay revealed that after 1 day of cell culture the metabolic activity of the cells seeded on the PEG-Dop/ Fe^{3+} /ox was the highest (see figure S12).

4. Discussion

The progress of extrusion printing for biomedical applications depends on the development of printable inks that allow ejection at low shear forces to be compatible with living cells, and show fast solidification after extrusion for good shape fidelity and stability of the printed constructs [4]. Systems with reversible bonds combined with a post-printing covalent crosslinking mechanism are suitable systems for this purpose [2, 4, 11, 12, 35, 36]. The reversible bonds lead to printable materials with favorable zero shear viscosities and shear thinning properties for printing. Post-printing covalent crosslinking allows mechanical stabilization of the printed features. Bioinspired catechol-based formulations, which can form reversible metal-coordinated bonds and can autocondensate to form a covalent network under mild oxidative conditions [37], are tested here as an example. Although metal-coordinated systems have been widely applied to many areas of materials science [37], they have only been rarely explored for biofabrication [3, 12, 16]. In this work, we have explored ink formulation and printing conditions of PEG-Dop polymers mixed with Al^{3+} , Fe^{3+} or V^{3+} ions. This system has been studied previously as dynamic, self-healing network [14, 15].

We identified a suitable formulation for printing consisting of 5% w/v PEG-Dop (10 kDa), 6,67 mM metal cation and 33 mM NaOH final concentrations. The polymer content is remarkably low compared to other printable PEG-based systems (e.g. 10% and 20% w/v PEG di-methacrylate [38], 25% w/v p(HPMA-m-lactate)-PEG [39], 5%–50% w/v PEG di-acrylate with alginate addition [40], 25% w/v PEG with 2.5% w/v alginate addition [41]). A viscoelastic network forms immediately after mixing with the metal ions, and remains stable in time. This is a profitable prerequisite for printing, as the ink can be prepared in advance to the fabrication process and used within few hours without losing its properties.

The properties of the metal coordination bond affect the rheological behavior and printing performance of the PEG-Dop/ M^{3+} ink. The tested metal-crosslinked inks (with Al^{3+} , Fe^{3+} and V^{3+}) allowed extrusion-based printing. Shear forces imposed during printing lead to reversible dissociation of the crosslinks and shear thinning properties, which facilitated extrusion. For good printability, the material has to flow through the nozzle and needs to undergo rapid (re)gelation just after ejection in order to maintain high shape fidelity of the printed structure [4]. Differences in printability were observed depending on the properties of the coordination complex used. Al^{3+} , Fe^{3+} and V^{3+} complexes with catechol group differ in the coordination degree at a given pH [15] and in the kinetic constant [28], but they show similar thermodynamic stability [26, 42] (table 2). The relaxation time (τ) of the network appeared to be the main parameter influencing the shape and the accuracy of the printed strand. The relaxation time reflects the dynamics and mobility of the network, and the ability to adopt the shape of the nozzle under the shear stress during printing [4, 43]. Well-defined strand deposition was possible with PEG-Dop/ Fe^{3+} and PEG-Dop/ Al^{3+} networks, with relaxation times below 1 s. PEG-Dop/ V^{3+} , with relaxation time around 40 s gave irregular structures (see figures 3(C), (D) and 4(D)), similar to those obtained when printing crosslinked gels [23]. By increasing the speed from 1 mm s^{-1} to 10 mm s^{-1} at a given printed pressure, stretched filaments were obtained for PEG-Dop/ Fe^{3+} and PEG-Dop/ Al^{3+} networks with relaxation time $< 1 \text{ s}$. The timescale at which rearrangements occur in the network should match the stretching rate imposed by the moving printing head. The longer τ of PEG-Dop/ V^{3+} did not allow for rearrangement in the crosslinking points and lead to breaking of the network during printing in wider range of conditions than for other inks. As a result, discontinuous filaments were obtained more easily. Strands from formulations with relaxation times $< 0.1 \text{ s}$, as in PEG-Dop/ Al^{3+} ink at pH 8.4, did not retain their shape before post-printing stabilization. In summary, PEG-Dop/ M^{3+} networks with relaxation times in the range of one to a few seconds present appropriate

balance between easiness of extrusion and good shape fidelity of printed strands, which retain the shape until post-printing stabilization by mild oxidative treatment.

The relaxation time of a metal-ligand crosslinked network is expected to be influenced by different parameters characteristic for metal-ligand coordination complex: the coordination degree, the ligand exchange kinetics and the thermodynamic stability constant. A higher coordination degree leads to longer relaxation time, since several ligands interact at the same crosslinking point with the metal cation [14, 15]. Reported studies at pH 8.0 demonstrated that the coordination degree of PEG-Dop/ M^{3+} networks decreased in the order of $V^{3+} > Fe^{3+} > Al^{3+}$ [15]. This trend is in agreement with the trend in the relaxation time of the materials observed in our study at pH 8.6–8.9. The coordination degree is expected to decrease with pH, as the ionization state of the catechol unit decreases. In agreement with this, PEG-Dop/ Al^{3+} formulation at pH 8.4 showed shorter relaxation times in comparison to the same formulation at pH 8.9. In a first approximation, we expect that the catechol exchange kinetic constant for a catechol/metal ion complex follows the same trend as reported water exchange constants for these complexes [44], i.e. $Al^{3+} < Fe^{3+} < V^{3+}$ (table 2). Faster kinetics of ligand exchange means more frequent dissociation (and association) of metal-catechol complexes, from which we expected faster network rearrangement [44]. This effect does not explain the longest relaxation time of PEG-Dop/ V^{3+} . The relation between relaxation times observed for PEG-Dop/ M^{3+} networks (PEG-Dop/ $V^{3+} > PEG-Dop/Fe^{3+} \approx PEG-Dop/Al^{3+}$) could be due to the counteracting effects of coordination degree and ligand exchange rate.

The printability differences observed between PEG-Dop/ Al^{3+} and PEG-Dop/ Fe^{3+} inks cannot be understood based on relaxation time argumentation. Therefore, we have measured the time needed for stiffness recovery after strain-induced breaking of the network (figure 2(D)). Recovery (self-healing) is possible due to the reversible nature of the metal complexes [3]. The observed trend in the recovery time PEG-Dop/ $V^{3+} \gg PEG-Dop/Fe^{3+} > PEG-Dop/Al^{3+}$ is expected to be related to the kinetic constant of the metal-ligand bond [27]. The water exchange kinetic constant decreases in the order $V^{3+} > Fe^{3+} \gg Al^{3+}$ (table 2), suggesting that this parameter explains only in part the observed recovery behavior. It was shown previously that Fe^{3+} drives catechol oxidation, which leads to introduction of some covalent crosslinks to the network [15, 45]. We suggest that a fraction of the covalent bonds is present in the PEG-Dop/ Fe^{3+} system in addition to transient metal-coordination crosslinks, as indicated by the (~ 2 fold) increased stiffness modulus of PEG-Dop/ Fe^{3+} network in comparison to other networks (figure 2(B)). The covalent bonds are expected to be irreversible, meaning very long kinetics, leading to purely covalent networks with only partial healing after breaking (figure S5, compare with [14, 33]). Therefore, recovery to a given percentage (see figure 2(D)) of the PEG-Dop/ Fe^{3+} network with

considerable fraction of covalent crosslinking can be expected to take longer, even though the recovery of the Fe^{3+} metal-ligand bonds is actually close to the V^{3+} time, as taken by the approximation from water-ligand exchange values.

Nevertheless, the general expected trend in recovery rate was observed for all the inks until 70% of the initial stiffness was reached (figures 2(D) and S2). At higher recovery ratio, deviations from this trend were observed for PEG-Dop/ Al^{3+} (pH 8.4) and PEG-Dop/ Fe^{3+} (20 kDa). PEG-Dop/ Al^{3+} at pH 8.4 recovered faster than expected based on the rate of ligand exchange, presumably due to the lower coordination degree. Faster recovery of PEG-Dop/ Fe^{3+} with higher molecular weight could be explained by the lower number of crosslinking points to be restored (1/2 of crosslinks number in 10 kDa PEG network) and the stronger influence of chain entanglements on the final material stiffness. The results suggest that the recovery of the PEG-Dop/ M^{3+} networks after strain-induced breaking mostly depends on the healing of bonds and re-formation of crosslinks at molecular scale and, therefore, it is dependent on the metal-ligand association rate and not on collective network dynamics (relaxation time), which seems to be more influenced by the metal coordination number. The experimental results suggest that PEG-Dop/ M^{3+} with quick recovery time (30% of recovery < 6 s) are profitable for shape fidelity. However, too quick recovery may lead to deposition of irregular stands, as in case of PEG-Dop/ V^{3+} , where full structural rearrangement and therefore well-defined cylindrical shape of strand, was not imposed while extrusion through the printing needle.

We now discuss the relationship between the properties of the coordination bond, the **viscosity** and the printability of the ink. The zero shear viscosity is the most commonly used parameter to characterize the bulk viscosity of shear-thinning polymeric materials [46]. Mathematical modeling of metal coordinated polymeric networks have demonstrated that the viscosity increases exponentially with the coordination degree (as the association of the polymeric chains increases), and decreases with increasing shear rate (shear thinning) as the crosslinks are forced to dissociate [47]. In the tested PEG-Dop/ M^{3+} inks, higher values of zero shear viscosity correlated with longer relaxation times and later end of non-Newtonian regime. Shear thinning effect appears above certain critical shear rate $\dot{\gamma}_c$, meaning end of non-Newtonian regime, and $\dot{\gamma}_c$ indicates terminal relaxation time of the polymer [47]. PEG-Dop/ V^{3+} had visibly later end of non-Newtonian regime than PEG-Dop/ Fe^{3+} and PEG-Dop/ Al^{3+} (figure 2(C)), which is in agreement with much longer relaxation time in comparison to the two other inks. The highest zero shear viscosity was observed for PEG-Dop/ V^{3+} , the ink with the highest coordination degree. PEG-Dop/ Al^{3+} and PEG-Dop/ Fe^{3+} showed comparable viscosity in the linear Newtonian regime, with slightly lower values for PEG-Dop/ Al^{3+} , and even

Table 4. Summary of literature-based relation between catechol-metal complexation chemistry and rheological parameters discussed in the study and recommended range of these values for good printing based on the study results.

	Associated with	Recommended values
Relaxation time	<ul style="list-style-type: none"> • degree of coordination [14, 15] • pH (degree of coordination and competition of HO- for binding sites) [14, 42] • k (kinetics of ligand exchange) [43, 44] 	~0,2 s
Recovery of 30%	<ul style="list-style-type: none"> • k (kinetics of ligand exchange) [44] 	1 s–6 s
Zero shear viscosity	<ul style="list-style-type: none"> • degree of coordination [47] • pH (degree of coordination and competition of HO- for binding sites) • k (kinetics of ligand exchange) [44] 	100–1000 Pa·s
Storage modulus	<ul style="list-style-type: none"> • log β (thermodynamics) [14, 34] • k (kinetics of ligand exchange) [42] • polymer molecular weight [49] 	Not relevant parameter in the presented system

lower for PEG-Dop/Al³⁺ (pH 8.4), indicating that in the system influence of coordination degree on viscosity was observed. The rate of bond dissociation/association is also expected to affect the response of the material to the applied shear. Therefore, viscosity is expected to be influenced by the ligand exchange rate constant: the faster the exchange rate, the higher viscosity. The trend in zero shear viscosity values (PEG-Dop/V³⁺ ≫ PEG-Dop/Fe³⁺ > PEG-Dop/Al³⁺) follows the order of ligand exchange kinetic constant (V³⁺ > Fe³⁺ ≫ Al³⁺). To conclude, viscosity influences the printing pressure and the resolution and accuracy of printing. Based on the obtained data, PEG-Dop/M³⁺ with zero shear viscosity in the range of 100–1000 Pa and showing shear thinning are printable.

Finally, we have observed differences in the elastic response of the inks tested at 10 Hz. PEG-Dop/Fe³⁺ showed higher elastic modulus than the PEG-Dop crosslinked with Al³⁺ or V³⁺ (see table S2). Reported data have related this effect to the higher stability constant (log β) of the complex [14, 34]. However, the difference in the stability constant between the metal-ligand pairs studied here are rather modest [26, 27]. It was shown previously that Fe³⁺ drives catechol oxidation, which leads to introduction of some covalent crosslinks to the network [15]. The fraction of covalent bonds could be accounted for the higher final stiffness of PEG-Dop/Fe³⁺ inks. The elastic behavior in PEG-Dop/M³⁺ networks is dominant at higher frequencies (above 0025 Hz for PEG-Dop/V³⁺, above ~5 Hz for PEG-Dop/Fe³⁺ and PEG-Dop/Al³⁺), but the behavior of the network at lower frequencies has a predominant influence on printing, i.e. post-printing stability. Therefore, in our system, the elastic modulus is not considered as relevant parameter. In crosslinked gel systems, where $G' > G''$, sufficient G' allows to keep the shape of printed form [48] and withstand the weight of consecutive layers. The parameters influencing material rheological properties and recommended values for good printability are collected in table 4.

Catechol-metal ligand crosslinking in PEG-Dop/M³⁺ inks resulted in the shear-thinning and self-healing properties beneficial for printing. However, the reversible character of metal-ligand crosslinking does not provide long-term stability of the printed structures. This is an inherent limitation of printable dynamic networks [4]. However, here the chemical versatility of the catechol group offers an additional advantage: a post-printing treatment under mild oxidative conditions allows covalent stabilization of the structures [5]. In this manner we obtained stable 3-dimensional printed structures. Printed filaments of PEG-Dop/Fe³⁺ ink gave the best outcome in terms of well-defined shape and resolution. For PEG-Dop/Al³⁺ the lower viscosity and poor shape fidelity observed in the 2D printing experiments hinder the construction of 3D structures. Well-printed 3D scaffolds with the PEG-Dop/V³⁺ were also successfully obtained, indicating that at larger scales the irregular shape of the filaments is no longer relevant. This highlights the importance of understanding the printing process and the ink parameters for the particular application.

PEG-Dop/Me³⁺ inks described in this article will guide the design of printable materials based on the catechol group. The inherent tunability of the catechol-metal complexes, and the versatile reactivity of the catechol unit will allow easy adaptation of ink properties to the needs of the printed structure.

As mussel-inspired catechol chemistry has been widely studied for biomedical materials and underwater adhesive formulations [5, 18], we have as well tested material biocompatibility. In the covalently crosslinked gels, we expect that the metal ions are partially depleted from the network due to the consumption of catechol chelating groups during oxidation. The non-bounded cations are expected to be removed, together with remaining oxidant, in the washing step preceding cell seeding on the casted materials. Additionally, previous studies have demonstrated toxic effects of Al³⁺ at 2 mM concentration, Fe³⁺ and V³⁺ at 1 mM, for fibroblasts after 48 h culture [50]. Note that the metal ion concentration in our study was below

1 mM (0.87 mM Me^{3+} concentration, assuming no metal ions removal in washing steps prior to cell seeding). The recommended daily intake for humans of Al, Fe and V ions is ca. 50 mg [51], 6–20 mg [52] and 1.8 mg [53], respectively. This amount would be enough to crosslink large volumes of the presented inks, i.e. 50 ml, 260 ml or 5 ml of the PEG-Dop/ Al^{3+} , / Fe^{3+} and / V^{3+} inks, respectively. Therefore, we expected no toxic effect of the formulations on the seeded cells. In short term studies (1 h cell contact with the network) indeed no toxicity effect was observed. Interestingly, in longer term, PEG-Dop/ Al^{3+} /ox and PEG-Dop/ Fe^{3+} /ox appeared to be biocompatible with the cells and induced cell proliferation, whereas PEG-Dop/ V^{3+} /ox material appeared to be toxic and non-suitable for biomedical application. Note, that for longer term studies addition of RGD cell adhesive domains to PEG-based networks is required [54–56]. Catechol units allow for straightforward material functionalization with RGD domains (for more details see SI), leading to well spread cell morphologies at later time points (day 4 and day 7). After 7 days of culture, over 70% of the PEG-Dop/ Al^{3+} /ox and PEG-Dop/ Fe^{3+} /ox gel surface was covered with spindle-shaped, well attached cells. We hypothesize that the observed low viability and proliferation of cells on the PEG-Dop/ V^{3+} /ox could be due to the lower efficiency of RGD functionalization of this formulation and to less effective depletion and washing of the V^{3+} ions from the network, with relatively higher toxic effect of these ions, as reported in literature.

Previous studies showed that addition of 4.5 mg ml^{-1} sodium periodate ($\sim 20 \text{ mM}$), to catechol-based hydrogels (final NaIO_4 concentration ca. 5 mM) during cell encapsulation caused negligible cytotoxicity *in vitro* and low immunogenicity *in vivo* [57]. As the NaIO_4 concentration used in our study was lower than reported for high viability culture [57], no toxicity induced by oxidant was expected even without a washing step. The obtained results indicate that the described printable PEG-Dop/ Al^{3+} and PEG-Dop/ Fe^{3+} inks are as well cytocompatible.

PEG-Dop/ Al^{3+} and PEG-Dop/ Fe^{3+} are suitable for acellular scaffolds production, and, followed by RGD functionalization, post-printing cell seeding. The use of proposed catechol groups makes necessary to use a working pH of 8.5–9 to allow for metal complexation, which precludes the inclusion of cells while printing. However, after further adjustment of the composition with different catechol derivatives [5] and RGD coupling in the material synthesis step, this limitation will be overcome and printing with embedded cells is envisioned. We foresee that PEG-Dop/ Me^{3+} , which reveals great tissue adhesive properties, as shown by us [18] and others for catechol-based biomaterials [58–60], can be especially useful as printable glues for fixing medical devices, or for tissue fixation in minimal surgery applications [11]. Adhesive printable formulations are currently very rare, but in high demand, as they facilitate

printing on tissues and direct fixation of the scaffold in desirable location, without need for additional gluing [11]. Additionally, great adhesive properties ensure good connection between printed layers and ensure scaffold integrity.

5. Conclusions

PEG-Dop/ M^{3+} based inks show several advantages for 3D extrusion printing. (i) They are reversible networks, with non-covalent crosslinks, that can be stabilized after printing by oxidant-triggered covalent reactions. (ii) The use of metal ions for crosslinking allows uncomplicated tuning of the material properties by metal exchange, facilitating the adaptation of the system to the requirements of particular printing process (broad range of printing parameters) and application with remarkable flexibility. (iii) We were able to obtain filaments with very good shape fidelity and resolution down to $150 \mu\text{m}$. Thinner filaments might be obtained using printing nozzles with smaller diameters. (iv) The PEG-Dop/ M^{3+} inks require low polymer content (final: 5%), following one of the most stringent criteria in bioink design [2]. (v) The crosslinking units (catechol) can be used for dynamic and covalent crosslinking, and applied to different polymeric systems. There is no need of additional crosslinking chemistries or UV-triggered reactions, which is the most common way to introduce post printing covalent crosslinking [35], but when not properly used may lead to cell damage. Additionally, different catechol derivatives can be applied, influencing network formation kinetics and environmental conditions (e.g. pH, oxidation) [5]. Although the proposed ink is not compatible with printing with embedded cells due to high pH of presented formulation (pH ~ 8.6), further ink optimization will allow to obtain bioinks with fast crosslinking kinetics at physiological pH and high cell compatibility.


The development of functional bioinks is a challenging task. Our results regarding the influence of crosslinking chemistry and reversible bond parameters on the rheological properties and printability of the ink provides fundamental understanding of the connection between materials chemistry, rheology and printing, and will guide material design in other reversible systems. We defined relaxation time and recovery time as main parameters indicating printability of ink with reversible bonds.

Acknowledgments

The authors thank Prof. Santiago J Garcia from the Faculty of Aerospace Engineering at the TU Delft, The Netherlands and Prof. Christian Wagner from Experimental Physics, Saarland University, Saarbrücken, Germany for the stimulating and fruitful discussions on rheological data. J F acknowledges the financial

support from China Scholarship Council. J I P, M V and A d C acknowledge financial support from the EU within BioSmartTrainee, the Marie Skłodowska-Curie Innovative Training School, No. 642861.


ORCID iDs

Małgorzata K Włodarczyk-Biegun  <https://orcid.org/0000-0003-1419-6166>

Julieta I Paez  <https://orcid.org/0000-0001-9510-7254>

Maria Villiou  <https://orcid.org/0000-0001-8966-3852>

Jun Feng  <https://orcid.org/0000-0001-7184-564X>

Aranzazu del Campo  <https://orcid.org/0000-0001-5725-2135>

References

- Ribeiro A, Blokzijl M M, Levato R, Visser C W, Castilho M, Hennink W E, Vermonden T and Malda J 2018 Assessing bioink shape fidelity to aid material development in 3D bioprinting *Biofabrication* **10** 014102
- Jos M, Jetze V, Melchels F P, Tomasz J, Hennink W E, Dhert W J A, Jürgen G and Huttmacher D W 2013 25th anniversary article: engineering hydrogels for biofabrication *Adv. Mater.* **25** 5011–28
- Zheng S Y, Ding H, Qian J, Yin J, Wu Z L, Song Y and Zheng Q 2016 Metal-coordination complexes mediated physical hydrogels with high toughness, stick-slip tearing behavior, and good processability *Macromolecules* **49** 9637–46
- Jungst T, Smolan W, Schacht K, Scheibel T and Groll J 2016 Strategies and molecular design criteria for 3D printable hydrogels *Chem. Rev.* **116** 1496–539
- Paez J I, Ustahüseyn O, Serrano C, Ton X-A, Shafiq Z, Auernhammer G K, d'Ischia M and del Campo A 2015 Gauging and tuning cross-linking kinetics of catechol-PEG adhesives via catecholamine functionalization *Biomacromolecules* **16** 3811–8
- Maccougall L J, Pérez-Madrigal M M, Arno M C and Dove A P 2018 Nonswelling thiol-yne cross-linked hydrogel materials as cytocompatible soft tissue scaffolds *Biomacromolecules* **19** 1378–88
- Paez J, Farrukh A, Włodarczyk-Biegun M K and del Campo A 2020 Thiol-methylsulfone based hydrogels for 3D cell encapsulation *ACS Appl. Mater. Interfaces* **12** 7
- Tabriz A G, Hermida M A, Leslie N R and Shu W 2015 Three-dimensional bioprinting of complex cell laden alginate hydrogel structures *Biofabrication* **7** 045012
- Wang L L, Highley C B, Yeh Y-C, Galarraga J H, Uman S and Burdick J A 2018 Three-dimensional extrusion bioprinting of single- and double-network hydrogels containing dynamic covalent crosslinks *J. Biomed. Mater. Res. Part A* **106** 865–75
- Highley C B, Rodell C B and Burdick J A 2015 Direct 3D printing of shear-thinning hydrogels into self-healing hydrogels *Adv. Mater.* **27** 5075–9
- Shin M, Galarraga J H, Kwon M Y, Lee H and Burdick J A 2019 Gallol-derived ECM-mimetic adhesive bioinks exhibiting temporal shear-thinning and stabilization behavior *Acta Biomater.* **95** 165–75
- Shi L, Carstensen H, Hölzl K, Lunzer M, Li H, Hilborn J, Ovsianikov A and Ossipov D A 2017 Dynamic coordination chemistry enables free directional printing of biopolymer hydrogel *Chem. Mater.* **29** 5816–23
- Krogsgaard M, Behrens M A, Pedersen J S and Birkedal H 2013 Self-healing mussel-inspired multi-pH-responsive hydrogels *Biomacromolecules* **14** 297–301
- Holten-Andersen N, Harrington M J, Birkedal H, Lee B P, Messersmith P B, Lee K Y and Waite J H 2011 pH-induced metal-ligand cross-links inspired by mussel yield self-healing polymer networks with near-covalent elastic moduli *Proc. Natl Acad. Sci.* **108** 2651–5
- Holten-Andersen N, Jaishankar A, Harrington M J, Fullenkamp D E, DiMarco G, He L H, McKinley G H, Messersmith P B and Lee K Y C 2014 Metal-coordination: using one of nature's tricks to control soft material mechanics *J. Mater. Chem. B* **2** 2467–72
- Li X, Wang H, Li D, Long S, Zhang G and Wu Z 2018 Dual ionically cross-linked double-network hydrogels with high strength, toughness, swelling resistance, and improved 3D printing processability *ACS Appl. Mater. Interfaces* **10** 31198–207
- Shi L, Zhao Y, Xie Q, Fan C, Hilborn J, Dai J and Ossipov D A 2018 Moldable hyaluronan hydrogel enabled by dynamic metal-bisphosphonate coordination chemistry for wound healing, advanced healthcare *Adv. Healthc. Mater.* **7** 1700973
- Feng J, Ton X-A, Zhao S, Paez J and del Campo A 2017 Mechanically reinforced catechol-containing hydrogels with improved tissue gluing performance *Biomimetics* **2** 23
- Diamantides N, Wang L, Pruiksmas T, Siemiatkoski J, Dugopolski C, Shortkroff S, Kennedy S and Bonassar L J 2017 Correlating rheological properties and printability of collagen bioinks: the effects of riboflavin photocrosslinking and pH *Biofabrication* **9** 034102
- Li H, Liu S and Lin L 2016 Rheological study on 3D printability of alginate hydrogel and effect of graphene oxide *Int. J. Bioprint.* **2** 54–66
- Li H, Tan Y J, Liu S and Li L 2018 Three-dimensional bioprinting of oppositely charged hydrogels with super strong interface bonding *ACS Appl. Mater. Interfaces* **10** 11164–74
- Li H J, Tan Y J, Leong K F and Li L 2017 3D bioprinting of highly thixotropic alginate/methylcellulose hydrogel with strong interface bonding *ACS Appl. Mater. Interfaces* **9** 20086–97
- Ouyang L, Yao R, Zhao Y and Sun W 2016 Effect of bioink properties on printability and cell viability for 3D bioplotting of embryonic stem cells *Biofabrication* **8** 035020
- Paxton N, Smolan W, Bock T, Melchels F, Groll J and Jungst T 2017 Proposal to assess printability of bioinks for extrusion-based bioprinting and evaluation of rheological properties governing bioprintability *Biofabrication* **9** 044107
- García-Fernández L et al 2013 Antibacterial strategies from the sea: polymer-bound cl-catechols for prevention of biofilm formation *Adv. Mater.* **25** 529–33
- Nurchi V M, Pivetta T, Lachowicz J I and Crisponi G 2009 Effect of substituents on complex stability aimed at designing new iron(III) and aluminum(III) chelators *J. Inorg. Biochem.* **103** 227–36
- Menyo M S, Hawker C J and Waite J H 2015 Rate-dependent stiffness and recovery in interpenetrating network hydrogels through sacrificial metal coordination bonds *ACS Macro Lett.* **4** 1200–4
- Helm L and Merbach A 2002 Applications of advanced experimental techniques: high pressure NMR and computer simulations *Chem. Soc., Dalton Trans.* **5** 633–41
- Sever M J and Wilker J J 2006 Absorption spectroscopy and binding constants for first-row transition metal complexes of a DOPA-containing peptide *Dalton Trans.* **813**–22
- Suntornnon R, Tan E Y S, An J and Chua C K 2016 A mathematical model on the resolution of extrusion bioprinting for the development of new bioinks *Materials* **9** 756
- Jin Y, Chai W and Huang Y 2017 Printability study of hydrogel solution extrusion in nanoclay yield-stress bath during printing-then-gelation biofabrication *Mater. Sci. Eng. C* **80** 313–25
- Webb B and Doyle B J 2017 Parameter optimization for 3D bioprinting of hydrogels *Bioprinting* **8** 8–12
- Li Q, Barrett D G, Messersmith P B and Holten-Andersen N 2016 Controlling hydrogel mechanics via bio-inspired polymer-nanoparticle bond dynamics *ACS Nano* **10** 1317–24
- Krogsgaard M, Hansen M R and Birkedal H 2014 Metals & polymers in the mix: fine-tuning the mechanical properties & color of self-healing mussel-inspired hydrogels *J. Mater. Chem. B* **2** 8292–7

- [35] Petta D, Grijpma D W, Alini M, Eglin D and D'Este M 2018 Three-dimensional printing of a tyramine hyaluronan derivative with double gelation mechanism for independent tuning of shear thinning and postprinting curing *ACS Biomater. Sci. Eng.* **4** 3088–98
- [36] Ouyang L, Highley C B, Rodell C B, Sun W and Burdick J A 2016 3D printing of shear-thinning hyaluronic acid hydrogels with secondary cross-linking *ACS Biomater. Sci. Eng.* **2** 1743–51
- [37] Wang B, Jeon Y S, Park H S, Kim Y J and Kim J-H 2015 Mussel-mimetic self-healing polyaspartamide derivative gel via boron-catechol interactions *EXPRESS Polym. Lett.* **9** 799–808
- [38] Cui X, Breitenkamp K, Finn M G, Lotz M and D'Lima D D 2012 Direct human cartilage repair using three-dimensional bioprinting technology *Tissue Eng. Part A* **18** 1304–12
- [39] Censi R, Schuurman W, Malda J, di Dato G, Burgisser P E, Dhert W J A, van Nostrum cf, di Martino P, Vermonden T and Hennink W E 2011 A printable photopolymerizable thermosensitive p(HPMAm-lactate)-PEG hydrogel for tissue engineering *Adv. Funct. Mater.* **21** 1833–42
- [40] Hockaday L A et al 2012 Rapid 3D printing of anatomically accurate and mechanically heterogeneous aortic valve hydrogel scaffolds *Biofabrication* **4** 035005
- [41] Hong S, Sycks D, Chan H F, Lin S, Lopez G P, Guilak F, Leong K W and Zhao X 2015 3D printing of highly stretchable and tough hydrogels into complex, cellularized structures *Adv. Mater.* **27** 4035–40
- [42] Menyo M S, Hawker C J and Waite J H 2013 Versatile tuning of supramolecular hydrogels through metal complexation of oxidation-resistant catechol-inspired ligands *Soft Matter* **9** 10314–23
- [43] Bose R K, Hohlbein N, Garcia S J, Schmidt A M and van der Zwaag S 2015 Connecting supramolecular bond lifetime and network mobility for scratch healing in poly(butyl acrylate) ionomers containing sodium, zinc and cobalt *Phys. Chem. Chem. Phys.* **17** 1697–704
- [44] Fullenkamp D E, He L, Barrett D G, Burghardt W R and Messersmith P B 2013 Mussel-inspired histidine-based transient network metal coordination hydrogels *Macromolecules* **46** 1167–74
- [45] Kim S, Peterson A M and Holten-Andersen N 2018 Enhanced water retention maintains energy dissipation in dehydrated metal-coordinate polymer networks: another role for Fe-catechol cross-links? *Chem. Mater.* **30** 3648–55
- [46] Hoare T, Zurakowski D, Langer R and Kohane D S 2010 Rheological blends for drug delivery. I. Characterization *in vitro* *J. Biomed. Mat. Res. A* **92** 575–85
- [47] Santo K P, Vishnyakov A, Kumar R and Neimark A V 2018 Elucidating the effects of metal complexation on morphological and rheological properties of polymer solutions by a dissipative particle dynamics model *Macromolecules* **51** 4987–5000
- [48] Chung J H Y, Naficy S, Yue Z, Kapsa R, Quigley A, Moulton S E and Wallace G G 2013 Bio-ink properties and printability for extrusion printing living cells *Biomaterials Science* **1** 763–73
- [49] Grindy S C, Lenz M and Holten-Andersen N 2016 Engineering elasticity and relaxation time in metal-coordinate cross-linked hydrogels *Macromolecules* **49** 8306–12
- [50] Hallab N J, Anderson S, Caicedo M, Brasher A, Mikecz K and Jacobs J J 2005 Effects of soluble metals on human peri-implant cells *J. Biomed. Mat. Res. A* **74A** 124–40
- [51] Krewski D, Yokel R A, Nieboer E, Borchelt D, Cohen J, Harry J, Kacew S, Lindsay J, Mahfouz A M and Rondeau V 2007 Human health risk assessment for aluminium, aluminium oxide, and aluminium hydroxide *J. Toxicol. Environ. Health B* **10** 1–269
- [52] Prasad K et al 2017 Metallic biomaterials: current challenges and opportunities *Materials* **10** 884
- [53] Becker S et al 2004 Opinion of the scientific panel on the dietetic products, nutrition and allergies [NDA] related to the tolerable upper intake level of vanadium *EFSA J.* **33** 1–22
- [54] Bakaic E, Smeets N M B and Hoare T 2015 Injectable hydrogels based on poly(ethylene glycol) and derivatives as functional biomaterials *RSC Adv.* **5** 35469–86
- [55] Kudva A K, Luyten F P and Patterson J 2018 RGD-functionalized polyethylene glycol hydrogels support proliferation and *in vitro* chondrogenesis of human periosteum-derived cells *J. Biomed. Mater. Res. A* **106** 33–42
- [56] Zhang C, Hekmatfer S and Karuri N W 2014 A comparative study of polyethylene glycol hydrogels derivatized with the RGD peptide and the cell-binding domain of fibronectin *J. Biomed. Mater. Res. A* **102** 170–9
- [57] Lee C, Shin J, Lee J S, Byun E, Ryu J H, Um S H, Kim D-I, Lee H and Cho S-W 2013 Bioinspired, calcium-free alginate hydrogels with tunable physical and mechanical properties and improved biocompatibility *Biomacromolecules* **14** 2004–13
- [58] Sedó J, Saiz-Poseu J, Busqué F and Ruiz-Molina D 2013 Catechol-based biomimetic functional materials *Adv. Mater.* **25** 653–701
- [59] Ryu J H, Lee Y, Kong W H, Kim T G, Park T G and Lee H 2011 Catechol-functionalized chitosan/pluronic hydrogels for tissue adhesives and hemostatic materials *Biomacromolecules* **12** 2653–9
- [60] Fan C, Fu J, Zhu W and Wang D-A 2016 A mussel-inspired double-crosslinked tissue adhesive intended for internal medical use *Acta Biomater.* **33** 51–63